Turbulence Analyses of Improved Electron Energy Confinement in H-Mode Plasmas with Gyrokinetic Calculations

Emi NARITA, Mitsuru HONDA[1)], Nobuhiko HAYASHI[1)], Tomonori TAKIZUKA, Shunsuke IDE[1)], Kiyoshi ITAMI[1)], Akihiko ISAYAMA[1)] and Takeshi FUKUDA

Graduate School of Engineering, Osaka University, Suita, Osaka 565-0871, Japan
[1)]*Japan Atomic Energy Agency, Naka, Ibaraki 311-0193, Japan*

(Received 24 February 2013 / Accepted 4 May 2013)

In the International Global H-mode Confinement Database, there are data that have the $H_{\mathrm{H98(y,2)}}$ factor exceeding unity in the region where the electron temperature is higher than the ion one. This high value of $H_{\mathrm{H98(y,2)}}$ can be attributed mainly to the improved electron confinement. The conditions required for this improvement are investigated with the local flux-tube gyrokinetic code GS2. When the ion temperature gradient length is shorter than the electron one, ion temperature gradient (ITG) mode is dominant, whereas trapped electron mode (TEM) is stabilized. Under this situation, the electron heat diffusivity is suppressed. In addition, an effect of the magnetic shear s is also studied in the positive shear range, $0.6 \leq s \leq 1.4$, and the reduction in the electron and ion heat transport with increasing s is found.

Keywords: energy confinement, turbulent transport, ITG/TEM transport, gyrokinetic code, temperature gradient, magnetic shear

DOI: 10.1585/pfr.8.1403082

1. Introduction

In burning plasmas, the electron temperature T_e is expected to be equal to or exceed the ion temperature T_i because of the electron heating due to alpha particles. It is, therefore, meaningful to investigate the effect of the temperature ratio $T_\mathrm{e}/T_\mathrm{i}$ on the plasma confinement for understanding transport in burning plasmas. In $T_\mathrm{e}/T_\mathrm{i} < 1$ region, the degradation of the confinement with the increase in T_e or $T_\mathrm{e}/T_\mathrm{i}$ has been generally observed [1]. In this region, the electron and ion thermal diffusivities increase with increasing $T_\mathrm{e}/T_\mathrm{i}$ [2]. The confinement degradation is attributed to the decrease in the ion temperature gradient (ITG) effective threshold due to the increase in $T_\mathrm{e}/T_\mathrm{i}$ [3,4]. The transport simulations showed that the increase in $T_\mathrm{e}/T_\mathrm{i}$ degrades the confinement in plasmas with the steep density gradient, because of the increase in ITG/trapped electron mode (TEM) transport [5]. However, in the International Global Confinement Database [1, 6], there are data that have the confinement enhancement factor $H_{\mathrm{H98(y,2)}}$ ($\equiv \tau_\mathrm{th}/\tau_{\mathrm{th,98y2}}$, where $\tau_{\mathrm{th,98y2}}$ is an ELMy H-mode confinement scaling expression since 1998 [7].) exceeding unity in $T_{\mathrm{e0}}/T_{\mathrm{i0}} > 1$ region, where $T_{\mathrm{e0}}/T_{\mathrm{i0}}$ is the temperature ratio at the magnetic axis [5]. The understanding of the underlying physics in a subset of these discharges can contribute to the improvement of the confinement and the precise prediction of the burning plasma performance.

In this paper, the electron and ion energy confinement performance of the subset are investigated. In this subset, it is found that the $H_{\mathrm{H98(y,2)}}$ factor exceeding unity can be attributed mainly to the improved electron confinement. In $T_\mathrm{e}/T_\mathrm{i} > 1$ region, ITG/TEM transport, which is enhanced with increasing $T_\mathrm{e}/T_\mathrm{i}$ as mentioned above, is analyzed using the GS2 code [8, 9] in order to investigate conditions required for the improved electron confinement. In the calculations, a role of the relationship between the electron and ion temperature gradient in turbulent transport is studied. The variances in the electron and ion temperature gradients were observed with the change in $T_\mathrm{e}/T_\mathrm{i}$ [4]. In addition, this study focuses on the dependence of transport on the magnetic shear relating to the plasma current shape, which impacts on the confinement quality.

The rest of this paper is organized as follows. Section 2 shows the data in $T_{\mathrm{e0}}/T_{\mathrm{i0}} > 1$ region of the International Global H-mode Confinement Database, and describes the improved electron confinement. In Sec. 3, the tools for analyzing turbulent transport are introduced. In addition to the linear calculations with the GS2 code, a quasilinear model is used to estimate the transport coefficients. The calculation results are also shown in Sec. 3. Section 4 gives the conclusions.

2. Improved Electron Confinement in the H-Mode Database

The International Global H-mode Confinement

author's e-mail: narita.emi@eb.see.eng.osaka-u.ac.jp

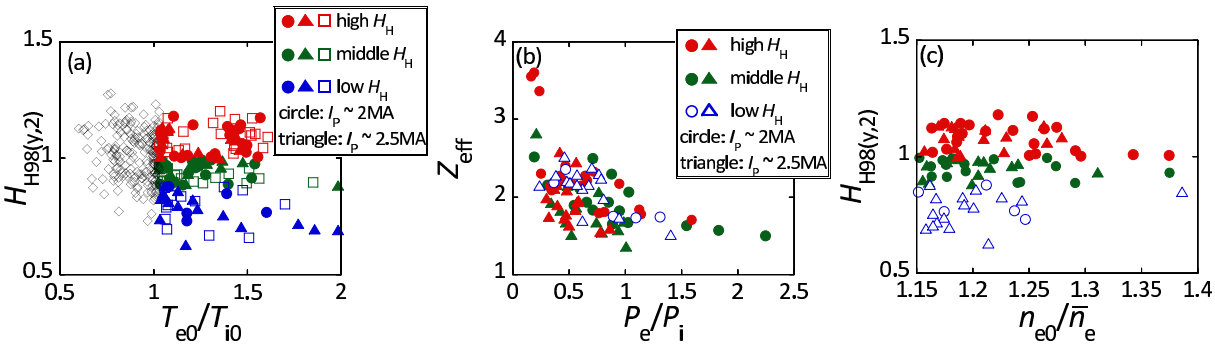

Fig. 1 (a) The plot of $H_{H98(y,2)}$ as a function of the temperature ratio at the magnetic axis. The data points in $T_{e0}/T_{i0} < 1.03$ are denoted by open diamonds, and the data points in $T_{e0}/T_{i0} > 1.03$ are divided in three groups: the high $H_{H98(y,2)}$ is in $H_{H98(y,2)} > 1$, the middle $H_{H98(y,2)}$ is in $0.88 < H_{H98(y,2)} < 1$ and the low $H_{H98(y,2)}$ is in $H_{H98(y,2)} < 0.88$. In $T_{e0}/T_{i0} > 1.03$, the subsets with the plasma current $I_p = 2$ MA and 2.5 MA are denoted by closed circles and closed triangles, and the remaining data points are denoted by open squares. The normal levels of accuracy of T_{e0} and T_{i0} are ±10% [6]. (b) The distribution of the NBI heating power ratio and the plasma effective charge. The symbols are corresponding to those in (a) except that the low $H_{H98(y,2)}$ data are denoted by open symbols. The normal level of accuracy of Z_{eff} is ±30% [6]. (c) The distribution of the ratio of the central electron density to the line averaged electron density and $H_{H98(y,2)}$. The symbols are corresponding to those in (b). The normal levels of accuracy of n_{e0} is ±10%, and that of $\bar{n}_e$ is ±8% [6].

Database [1, 6] was surveyed with an emphasis on the dependence of $H_{H98(y,2)}$ on T_{e0}/T_{i0}, and the degradation of $H_{H98(y,2)}$ with the increase in T_{e0}/T_{i0} under the steep density gradient was suggested [5]. The transport simulations showed that the degradation can be attributed to enhanced ITG/TEM turbulence [5]. In this section, we investigate a subset of the database DB3v13 [1, 6] to study the data that have $H_{H98(y,2)}$ exceeding unity in $T_{e0}/T_{i0} > 1$ region. The data points from JET discharges have been extracted from the database, because these discharges consist of enough shots with the plasmas of T_e/T_i exceeding unity. The data points are scattered over broad range of T_{e0}/T_{i0} as shown in Fig. 1 (a). All data selected here are the ELMy H-mode discharges with deuterium plasmas dominantly heated by neutral beam injection (NBI). The discharges with pellet injection are excluded from the subset. The safety factor at 95% flux surface q_{95} falls within $2.8 < q_{95} < 4.5$, and the line averaged electron density $\bar{n}_e$ and the central electron density n_{e0} range $0.3 < \bar{n}_e/n_{GW} < 0.8$ and $1.15 < n_{e0}/\bar{n}_e < 1.4$, respectively, where n_{GW} is the Greenwald density ($n_{GW}(10^{20}\,\mathrm{m}^{-3}) \equiv I_p/\pi a^2$, where I_p is the plasma current in units of MA and a is the plasma minor radius in m). This study focuses on the data points within $T_{e0}/T_{i0} > 1.03$ region in Fig. 1 (a). As described in Fig. 1 (a), the data in this region are divided in the three groups based on $H_{H98(y,2)}$: the high $H_{H98(y,2)}$ is in $H_{H98(y,2)} > 1$, the middle $H_{H98(y,2)}$ is in $0.88 < H_{H98(y,2)} < 1$ and the low $H_{H98(y,2)}$ is in $H_{H98(y,2)} < 0.88$. The NBI heating power ratio P_e/P_i, which is not contained within the database, is calculated with the following equation [10]:

$$\frac{dE_b}{dt} = -P_{E_b,i} - P_{E_b,e} \quad (1)$$

$$= -\frac{2E_b}{\tau^{b/i}} \quad (2)$$

$$- \frac{2E_b}{\tau^{b/e}}\left[\left(\frac{E_b}{T_{e,Vol}} - \frac{3}{2}\right)\left(\frac{mE_b}{MT_{e,Vol}}\right)^{1/2}\frac{4}{3\sqrt{\pi}}\right], \quad (3)$$

and therefore P_e/P_i is estimated as

$$\frac{P_e}{P_i} = \frac{\displaystyle\int_{T_{e,Vol}}^{E_{b0}} \frac{2E_b}{\tau^{b/e}}\left[\left(\frac{E_b}{T_{e,Vol}} - \frac{3}{2}\right)\left(\frac{mE_b}{MT_{e,Vol}}\right)^{1/2}\frac{4}{3\sqrt{\pi}}\right] dE_b}{\displaystyle\int_{T_{e,Vol}}^{E_{b0}} \frac{2E_b}{\tau^{b/i}}\, dE_b}, \quad (4)$$

where E_b is the energy of fast ions produced by the neutral beam, E_{b0} is the neutral beam energy, $P_{E_b,i(e)}$ is the power transferred from the fast ions to thermal ions (electrons), $T_{e,Vol}$ is the volume averaged electron temperature expressed as

$$T_{e,Vol} = \frac{W_e}{\frac{3}{2}n_{e,Vol}V}, \quad (5)$$

W_e is the electron stored energy, $n_{e,Vol}$ is the volume averaged electron density, V is the plasmas volume, m is electron mass, M is deuterium mass and $\tau^{b/i}$ and $\tau^{b/e}$ are energy transfer time from fast ions to thermal ions and to electrons respectively, which are evaluated as $\tau^{b/e} \propto E_b^{3/2}$ and $\tau^{b/i} \propto E_b^{3/2}/Z_{eff}$ (where Z_{eff} is the line averaged plasma effective charge). The parameter ranges of P_e/P_i and Z_{eff} for the high, middle and low $H_{H98(y,2)}$ are shown in Fig. 1 (b), in which the subset of the discharges with $I_p = 2$ MA and 2.5 MA is selected. Special relationships of the range of P_e/P_i and Z_{eff} to $H_{H98(y,2)}$ are not seen. Although P_e/P_i is estimated roughly using the volume averaged value of the temperature, the poor relationship between P_e/P_i and $H_{H98(y,2)}$ can be confirmed, and the most P_e/P_i values range under unity. A exact estimate of P_e/P_i will be performed with radially resolved simulation in the future. In

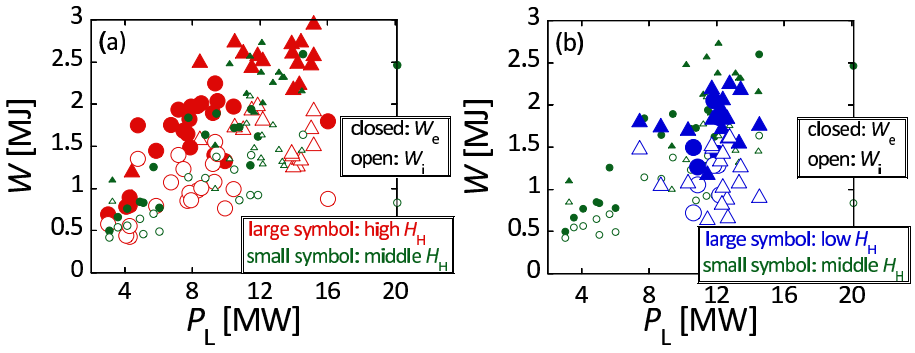

Fig. 2 The dependence of the stored energy on the loss power using the data with (a) high (large symbols) and middle (small symbols) $H_{H98(y,2)}$ and (b) low (large symbols) and middle (small symbols) $H_{H98(y,2)}$. Closed and open symbols denote the electron and ion energy, respectively, and circle and triangle symbols denote the data with plasma current $I_p = 2$ MA and $I_p = 2.5$ MA, respectively. The normal level of accuracy of W_e is ±20%, and that of W_i is ±15% [6].

Fig. 1 (c), $H_{H98(y,2)}$ is plotted versus the density peaking factor $n_{e0}/\bar{n}_e$. The density gradient does not affect the $H_{H98(y,2)}$. Figure 2 shows the dependence of the stored energies of electrons W_e and ions W_i on the loss power P_L evaluated by subtracting the time rate of change in the total plasma stored energy from the sum of the ohmic and auxiliary heating power. In the data set of the high $H_{H98(y,2)}$ (shown in Fig. 2 (a)) the increases in W_e and W_i are seen more clearly than those in the data set of low $H_{H98(y,2)}$ (shown in Fig. 2 (b)). Figure 2 (a) also shows that W_e is nearly twice larger than W_i. Thus, the increase in $H_{H98(y,2)}$ can be attributed mainly to the improvement of the electron energy confinement. In the next section, the influence of the difference between the electron and ion temperature gradients on the electron confinement is investigated, because the stored energy ratio W_e/W_i is larger than the temperature ratio at the magnetic axis T_{e0}/T_{i0}, and the electron temperature gradient length may be longer than the ion one. In addition, we consider an effect of the current density profile, which has been generally reported to be significant for the confinement performance [11, 12]. Since the confinement performance is compared for the high, middle and low $H_{H98(y,2)}$ cases with the similar plasma current, the current density profile may influence the improved electron confinement. Accordingly, in the next section, roles of the electron and ion temperature gradient length and the magnetic shear indicating the current density profile are studied in the $T_e/T_i > 1$ region for the fixed density gradient value.

3. Turbulence Analyses

In order to study a mechanism of the improved electron energy confinement observed in the database, the electron and ion thermal transport induced by turbulence are investigated with the GS2 code [8,9]. In the following subsection, the calculation methodologies are shown.

3.1 Methodologies

GS2 is the local flux-tube gyrokinetic code, and solves the gyrokinetic equations for the perturbed distribution function δf. In this paper, the linear calculations are performed mainly, including electromagnetic effects. The $s - \alpha$ equilibrium model [13] is employed because the parameters required for this model are available from the International Multi-Tokamak Confinement Profile Database [14], whereas some parameters needed for the Miller equilibrium model [15], which can also be used in GS2 calculations, are not available in the database. Here, s is the magnetic shear and α is the normalized pressure gradient. The heat transport coefficients are estimated based on linear calculations using a quasilinear transport model [16]. This model is applicable for ITG and TEM turbulence, and in the case where turbulence tends to be mainly driven by ITG mode, the ion heat flux Q_i is estimated as

$$\frac{Q_i}{n_i T_i / R} = C \max_{k_\theta} \left[\frac{\gamma}{\left\langle k_\perp^2 \right\rangle} \right] \frac{R}{L_{T_i}}. \tag{6}$$

Here, n_i is the ion density, R is the major radius, γ is the linear growth rate, k_θ is the wave number in the poloidal direction, $k_\perp$ is the perpendicular wave number and L_{T_i} is the ion temperature gradient length defined by $L_{T_i} = -T_i/\nabla T_i$. The dimensionless factor C, which is determined by nonlinear simulations, is set to unity for our cases. The validity of the C value will be discussed bellow. The poloidal average value of $k_\perp^2$ is defined as

$$\left\langle k_\perp^2 \right\rangle = k_\theta^2 \left(1 + s^2 \left\langle \theta^2 \right\rangle \right), \tag{7}$$

where

$$\left\langle \theta^2 \right\rangle \equiv \frac{\int \theta^2 \left| \phi_{k_\theta}(\theta) \right|^2 \mathrm{d}\theta}{\int \left| \phi_{k_\theta}(\theta) \right|^2 \mathrm{d}\theta}. \tag{8}$$

Here, ϕ_{k_θ} is the fluctuating potential. The calculations are performed in the range of $0.1 < k_\theta \rho_i < 1.0$, where $\rho_i = c_s/\Omega_i$ with $c_s = (T_e/M)^{0.5}$ and $\Omega_i = eB/M$. As described in Eq. (6), the heat flux is estimated by the maximum value

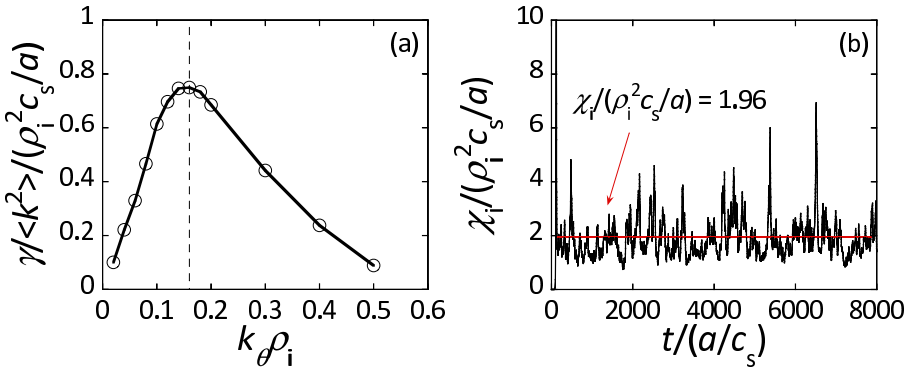

Fig. 3 (a) Linear calculation result of $\gamma/\left\langle k_\perp^2\right\rangle$ in Eq. (6) as a function of the normalized wave number, and (b) nonlinear simulation result of the time trace of the ion heat diffusivity for Cyclone base case parameters.

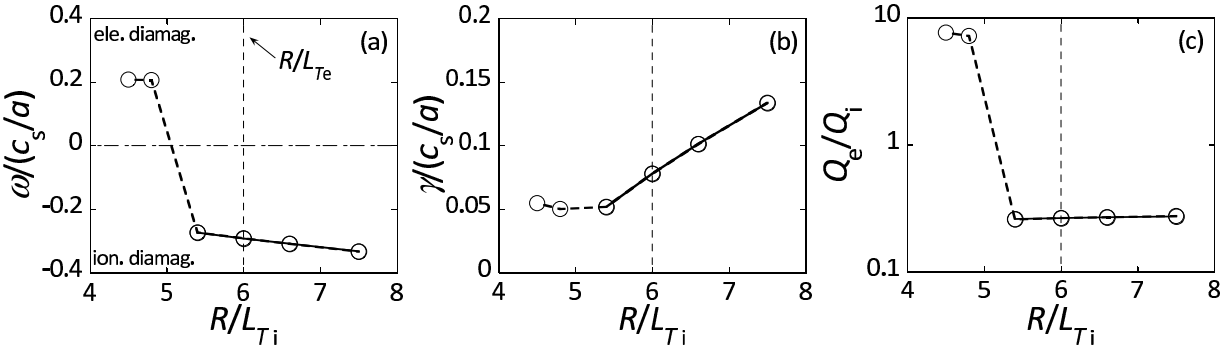

Fig. 4 (a) The mode frequency, (b) the linear growth rate and (c) the heat flux ratio as a function of the normalized ion temperature gradient, with $R/L_{T_e} = 6$ and $k_\theta\rho_i = 0.3$. The dotted vertical line shows the value of $R/L_{T_e} = 6$ kept fixed in the calculations.

of the $\gamma/\left\langle k_\perp^2\right\rangle$ over the $k_\theta\rho_i$ range, and the maximum value is generally taken around $k_\theta\rho_i \sim 0.1 - 0.15$. The ion heat diffusivity χ_i is calculated using $Q_i = -n_i\chi_i\nabla T_i$, and thus

$$\chi_i = C \max_{k_\theta}\left[\frac{\gamma}{\left\langle k_\perp^2\right\rangle}\right]. \tag{9}$$

The electron heat diffusivity χ_e is subsequently computed using the heat diffusivity ratio χ_e/χ_i calculated from the heat flux ratio Q_e/Q_i that is the result of linear calculations. In the case where the dominant turbulence drive is TEM, the roles of ion and electron would be interchanged with each other and thus the subscript "i" is replaced with "e" in Eq. (6) and Eq. (9).

The quasilinear model, Eq. (9), includes the dimensionless factor C. In order to determine the factor C, the nonlinear simulation of electrostatic ITG turbulence is performed, and the result is compared with that from the linear calculation. The plasma parameters are identical to the Cyclone base case [17] ($r/R = 0.18$, $s = 0.8$, $q = 1.4$, $R/L_n = 2.2$, $R/L_{T_i} = 6.9$ and $T_e/T_i = 1$). The electrostatic calculation for these parameters is widely used for a benchmark case. In the nonlinear simulation, the box sizes in the x and y directions are $L_x = L_y = 62.8\rho_s$, respectively, where x is the radial direction and y is the perpendicular direction to the field line. Figures 3 (a) and 3 (b) show the linear and nonlinear results, respectively. The ion heat diffusivity χ_i shown in Fig. 3 (b) is calculated from the ion heat flux Q_i that is the nonlinear simulation result. Both $\gamma/\left\langle k_\perp^2\right\rangle$ and χ_i are normalized to $\rho_i^2 c_s/a$. The normalized maximum value of $\gamma/\left\langle k_\perp^2\right\rangle$ is 0.750, and the normalized time averaged χ_i is 1.96, then $C = 2.61$ is obtained. Assuming C to be of order unity is, therefore, justified.

3.2 Results

In Sec. 2, it is concluded that the $H_{H98(y,2)}$ factor exceeding unity in the high T_{e0}/T_{i0} region can be attributed mainly to the improved electron confinement. In this subsection, conditions required for the improvement in the high T_e/T_i region are investigated by means of the linear stability calculations with GS2. In the comparison of the stored energy for the high, middle and low $H_{H98(y,2)}$ as shown in Fig. 2, it is speculated that the electron and ion temperature gradients and the magnetic shear influence the difference in the $H_{H98(y,2)}$ value. These influences on ITG/TEM turbulence, which is reported to be enhanced in the high T_e/T_i region, are examined. Here, $T_e/T_i = 1.2$ is selected as a representative of high T_e/T_i.

Figure 4 shows the effect of the normalized ion tem-

perature gradient R/L_{T_i} on ITG/TEM turbulence with $T_e/T_i = 1.2$ and the normalized electron temperature gradient $R/L_{T_e} = 6$, at $k_\theta\rho_i = 0.3$ around which ITG/TE mode has the maximum growth rate γ. At the wave number lies within $0.1 < k_\theta\rho_i < 0.15$, in which $\gamma/\langle k_\perp^2 \rangle$ is the maximum, the effect of the ion temperature gradient on turbulence is in a similar manner to at $k_\theta\rho_i = 0.3$. The mode frequency ω and γ are normalized to c_s/a, and the positive (negative) ω indicates the propagation in the electron (ion) diamagnetic direction. The $\rho_i^2 c_s/a$ value used for the normalization of the heat diffusivity given in Eq. (9) is calculated by the typical values in the subset in the previous section: $B = 2.3$ T, $a = 0.93$ m and $T_{e,Vol} = 2.2$ keV. Here, the plasma parameters are $R/a = 3$, $r/a = 0.5$, $\beta = 0.5\%$, $s = 1.0$, $q = 1.5$ and $R/L_n = 2$, where r/a is the normalized minor radius, β is the ratio of the plasma pressure to the magnetic energy density, q is the magnetic safety factor and R/L_n is the normalized density gradient. These values are set based on discharges in the International Multi-Tokamak Confinement Profile Database [14], which are the part of the data points in Fig. 1 (a). The α parameter is set to zero. As shown in Fig. 4 (a), when R/L_{T_i} is larger than ~ 5, the dominant mode is ITG, on the other hand, when R/L_{T_i} is less than ~ 5, TEM is the fastest growing mode. This ITG/TEM transition associated with R/L_{T_i} is observed in Ref. [18–20]. In Ref. [19, 20], the transition occurs at $R/L_{T_i} \sim C_t R/L_{T_e}$, where C_t varies around unity according to other parameters. In this study, C_t is slightly lower than unity. In order to study the sensitivity of C_t to s and R/L_{T_e}, variations of s and R/L_{T_e} by ±20% are examined, accounting experimental errors. C_t has an error within ±10% with the R/L_{T_e} variation, and an error within ±9% with the s variation. C_t does not exceed unity with these variations. The linear growth rate is enhanced by the increase in R/L_{T_i} (Fig. 4 (b)), but in the ITG-dominated regime, namely in $R/L_{T_i} > 5$, the electron heat flux is much less than the ion one, as shown in Fig. 4 (c). Figure 5 shows the heat diffusivities estimated by the quasilinear transport model. The closed and open circles denote the electron and ion heat diffusivities with $R/L_{T_e} = 6$, respectively. In a condition $R/L_{T_i} > 5$, ITG is the fastest growing mode, and the electron heat diffusivity is much less than the ion one, whereas when the dominant turbulence drive is TEM, it is enhanced substantially and exceed the ion heat diffusivity. As shown in previous section, in the data set of the high $H_{H98(y,2)}$, W_e is significantly larger than W_i. In order to obtain this situation, the regime where TEM is suppressed and ITG is dominant is required. In TEM-dominated regime ($R/L_{T_i} < 5$), χ_i increases slightly with decreasing R/L_{T_i} (open circles in Fig. 5). The open triangles in Fig. 5 show the χ_i driven by pure ITG mode with $R/L_{T_e} = 0$. The other parameters are identical to those used for circle symbols. The pure ITG mode is suppressed with decreasing R/L_{T_i}. Therefore, the slight increase in χ_i is due to TEM. This role of TEM is suggested in the experiments [20]. In Fig. 6, the dependence of χ_e, χ_i and

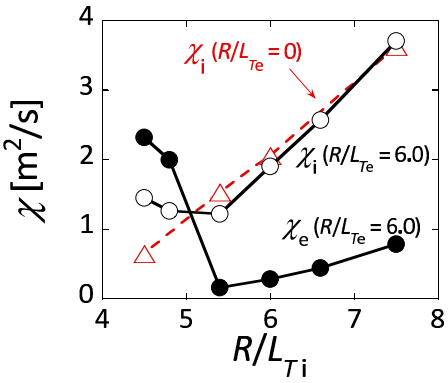

Fig. 5 Quasilinear estimate of the heat diffusivities of electrons (closed symbols) and ions (open symbols) for the fixed value of $R/L_{T_e} = 6$, and the ion heat diffusivity driven by the pure ITG mode with $R/L_{T_e} = 0$ denoted by open triangles as a function of the normalized ion temperature gradient.

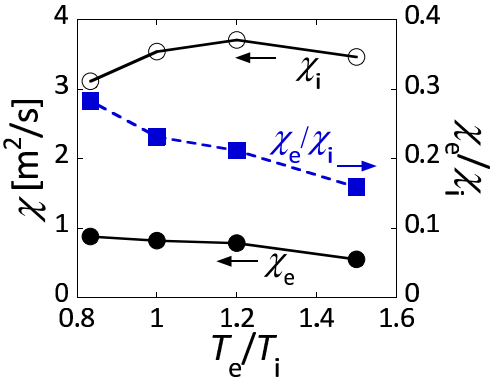

Fig. 6 Quasilinear estimate of the heat diffusivities of electrons (closed circles) and ions (open circles), and linear calculation result of the heat diffusivity ratio (closed squares) as a function of the temperature ratio.

χ_e/χ_i on T_e/T_i is plotted with the parameters that are identical to those used previously except for $R/L_{T_e} = 6.0$ and $R/L_{T_i} = 7.5$. For any T_e/T_i, the mode frequency is negative, meaning that the fastest growing mode is ITG mode. With increasing T_e/T_i, χ_e and χ_e/χ_i gradually decrease, whereas χ_i increases. In this range of T_e/T_i, since χ_e is less than χ_i, a condition $R/L_{T_i} > R/L_{T_e}$ is effective for the reduction in the electron heat transport. In the subset with the high $H_{H98(y,2)}$ of the database, since W_e/W_i is larger than T_{e0}/T_{i0}, the electron temperature profile can be broader and the electron temperature gradient can be smaller: $R/L_{T_i} > R/L_{T_e}$. This range corresponds to the region where χ_e is much lower than χ_i. Therefore, the calculation results support the above speculation.

The effect of the magnetic shear on the electron energy confinement is also examined. The mode frequency and the linear growth rate as a function of $k_\theta\rho_i$ for $s = 1.4, 1.0$ and 0.6, with $T_e/T_i = 1.2$, $R/L_{T_e} = 6$ and $R/L_{T_i} = 7.5$,

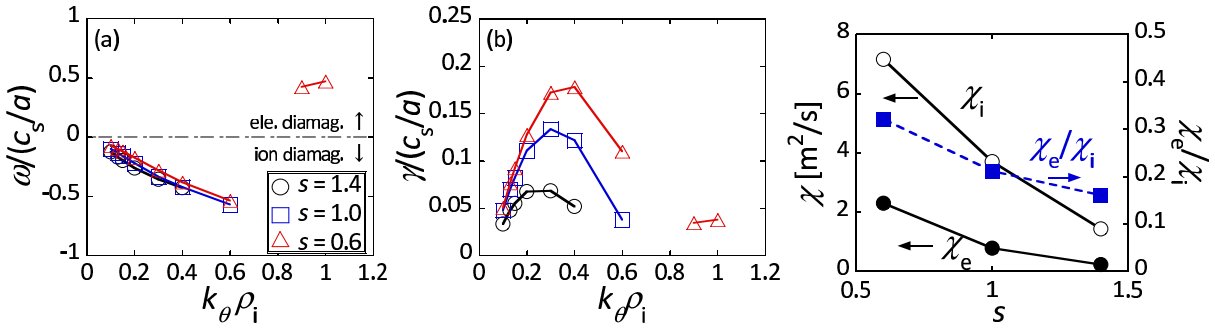

Fig. 7 (a) The mode frequency and (b) the linear growth rate versus the normalized wave number for the magnetic shear $s = 1.4$ (circle symbols), $s = 1.0$ (square symbols), and $s = 0.6$ (triangle symbols). (c) Quasilinear estimate of the heat diffusivities of electrons (closed circles) and ions (open circles), and linear calculation result of the heat diffusivity ratio (closed squares) as a function of s.

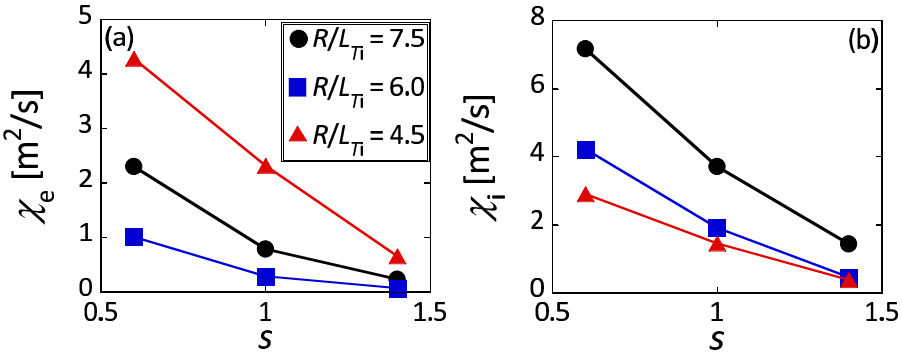

Fig. 8 Quasilinear estimate of (a) the electron heat diffusivity and (b) the ion heat diffusivity as a function of the magnetic shear for the normalized ion temperature ratio $R/L_{T_i} = 7.5$ (circle symbols), $R/L_{T_i} = 6.0$ (square symbols) and $R/L_{T_i} = 4.5$ (triangle symbols), with a fixed value of $R/L_{T_e} = 6.0$.

are shown in Fig. 7 (a) and Fig. 7 (b), respectively. Around $k_\theta\rho_i \sim 0.7$, the dominant instability shifts from ITG to TEM (Fig. 7 (a)). As shown in Fig. 7 (b), both ITG and TEM turbulence is suppressed by the increase in s. Figure 7 (c) shows the estimated heat diffusivities. χ_e/χ_i decreases with increasing in s, hence the increase in s reduces χ_e faster than χ_i. The reductions in χ_e and χ_i are observed for the other value of R/L_{T_i} with a fixed value of $R/L_{T_e} = 6$ as shown in Fig. 8. For any s, when $R/L_{T_i} = 7.5$ and 6, the dominant mode is ITG, whereas when $R/L_{T_i} = 4.5$, TEM becomes dominant. TEM turbulence causes the increase in χ_e (triangles in Fig. 8 (a)), as mentioned before. χ_e and χ_i decrease with increasing in s clearly. The stabilizing dependence on s was given in [21], which analyzed the ion temperature gradient driven mode of a sheared slab model. The linear analysis showed that the growth rate is approximately a decreasing function of s, and the reduction in χ_i of the mode with increasing s is observed from the fully nonlinear simulation [21]. The increase in s for the range selected in this study was also reported to reduce the electron and ion transport with the equal ion temperature gradient to the electron one using gyrokinetic code GYRO [11].

3.3 Discussion on results

The validity of the low heat diffusivity ratio χ_e/χ_i calculated by GS2 is also examined in terms of the experiments. The GS2 calculations show that χ_e is significantly lower than χ_i, in the case where R/L_{T_i} is sufficient large to shift the dominant mode to ITG, and high s in the positive shear range. This low χ_e can improve the electron confinement. In the subset of the high $H_{H98(y,2)}$ shown in Sec. 2, the electron stored energy is nearly twice larger than the ion one. In this subset, the NBI power transferred to electrons is less than that to ions as shown in Fig. 1 (b). The validity of the low χ_e compared to χ_i with $P_e/P_i < 1$ is investigated with the electron and ion energy balance equations expressed in the following form [22]:

$$\frac{W_e}{\tau_{E,e}} = P_e - \frac{T_e - T_i}{\tau_{eq}} n_e V, \tag{10}$$

$$\frac{W_i}{\tau_{E,i}} = P_i + \frac{T_e - T_i}{\tau_{eq}} n_e V, \tag{11}$$

where $\tau_{E,e(i)}$ is the electron (ion) energy confinement time, V is the plasma volume and τ_{eq} is the equipartition time expressed as

$$\tau_{eq} = \frac{1}{3}\tau_e \frac{M}{m}. \tag{12}$$

Here the electron collision time τ_e is written as

$$\tau_e = \frac{3.5 \times 10^4}{\ln \Lambda_e / 10} \frac{T_e^{3/2}}{Zn}, \quad (13)$$

where $\ln \Lambda_e$ is the Coulomb logarithm, and the units of T_e and n is eV and cm^{-3}, respectively. When we assume $\chi_e \ll \chi_i$, the outflux of electron energy is nearly zero: $W_e/\tau_{E,e} = 0$ in Eq. (10). In addition, the ratio of P_e in Eq. (10) to P_i in Eq. (11) varies from $P_e/P_i = 0.5$ to $P_e/P_i = 1.0$. Under these assumption, the value of T_e/T_i is calculated by Eq. (10) and Eq. (11). Here, the following characteristic values in the subset of the database are used: $T_{e,Vol} = 2.2\,keV$, $n_e = 4.1 \times 10^{19}\,m^{-3}$, $W_e = 1.8\,MJ$, $W_i = 1.1\,MJ$ and $\tau_E = 350\,ms$, where τ_E is expressed as $\tau_E = \tau_{E,i}(W_e + W_i)/W_i$ because $W_e/\tau_{E,e} = 0$ is assumed. Consequently, for $P_e/P_i = 0.5 - 1.0$, $T_e/T_i = 1.2 - 1.3$ is obtained. This obtained T_e/T_i lies within the range given in the subset of the database. It means that when the electron heat transport has been suppressed significantly, the balance between the electron heating and the equipartition energy flow to ions can be kept.

4. Conclusions

In the International Global Confinement Database, the electron and ion confinement properties of the data in $T_{e0}/T_{i0} > 1$ region have been investigated. The data points from JET discharges show that $H_{H98(y,2)}$ exceeding unity can be attributed mainly to the improved electron confinement. The conditions required for this improvement in $T_e/T_i > 1$ region have been investigated with the linear GS2 calculations, focusing on the electron and ion temperature gradients and the magnetic shear in the high T_e/T_i region, because these are suggested to influence the improved electron confinement in the data set. The heat diffusivities have been estimated using the quasi-linear model. The ion temperature gradient has varied while keeping electron temperature gradient fixed. When R/L_{T_i} is larger than R/L_{T_e}, the fastest growing mode is ITG, and the increase in R/L_{T_i} enhances the linear growth rate. Under this condition, the value of χ_e is less than that of χ_i. At $R/L_{T_i} \sim C_t R/L_{T_e}$, the ITG/TEM transition occurs. For the parameter set given in this paper, C_t is slightly lower than unity. In the TEM-dominated regime, the electron transport is enhanced. The T_e/T_i scan shows that when ITG mode is dominant, χ_e is kept much lower than χ_i in $T_e/T_i > 1$ region. Consequently, a condition $R/L_{T_i} > R/L_{T_e}$ is required for the reduction in the electron heat transport. The range $R/L_{T_i} > R/L_{T_e}$, which is suggested in the subset, corresponds to the region where χ_e is much lower than χ_i. In addition, the study of the magnetic shear effect on the heat transport in the positive shear range, $0.6 \le s \le 1.4$, shows that the increase in s reduces both χ_e and χ_i, and the reduction in χ_e is larger than that in χ_i. As shown by the calculations, when the electron transport is suppressed, χ_e is much lower than χ_i. The validity of the low χ_e/χ_i has been examined in terms of the experiments by the energy balance equations. The significant reduction of χ_e can be occur within the high T_e/T_i range given in the subset of the database. The temperature gradients and the magnetic shear affect the improved electron confinement, and thus, these calculations support the suggestion in the subset of the database.

In this study, the GS2 calculations have been performed with the $s - \alpha$ equilibrium model [13]. However, it has been reported that the results are different between the $s - \alpha$ model and a magnetohydrodynamic (MHD) equilibrium: for the case with the $s - \alpha$ model, the linear growth rate is underestimated and the ITG critical gradient is overestimated [23]. In this study, χ_e and χ_i have been investigated with respect to the temperature gradient ratio and the magnetic shear in the low-k region by the local flux-tube code, but the electron temperature gradient (ETG) mode originating at high wave numbers ($k_\theta \rho_i > 1$) provides a small but important effect on the electron transport [24, 25]. This work will be extended to high-k turbulence in due course. Also, experimental analyses will be performed in JT-60U to see whether the electron transport characteristics captured in this study are reproduced. In addition, simulations with the integrated transport code TOPICS [26] implementing the transport models GLF23 [27] and TGLF [28] will be carried out, and in these simulations, turbulent transport, kinetic profiles and an equilibrium are consistent with each other.

Acknowledgments

The authors would like to thank Dr K. Tanaka of National Institute for Fusion Science for helpful discussions on the GS2 code. One of the authors (E.N.) also thanks Drs Y. Kamada and T. Fujita for their fruitful discussions and continuous encouragement during her stay in JAEA as a fellow of advanced science. This work was carried out using the HELIOS supercomputer system at International Fusion Energy Research Centre, Aomori, Japan, under the Broader Approach collaboration between Euratom and Japan, implemented by Fusion for Energy and JAEA.

[1] Progress in the ITER Physics Basis, Chapter2: Plasma confinement and transport, Nucl. Fusion **47**, S18 (2007).
[2] C.C. Petty *et al.,* Phys. Rev. Lett. **83**, 3661 (1999).
[3] J. Weiland *et al.,* Plasma Phys. Control. Fusion **47**, 441 (2005).
[4] A. Manini *et al.,* Nucl. Fusion **46**, 1047 (2006).
[5] E. Narita *et al.,* Plasma Fusion Res. **7**, 2403102 (2012).
[6] The International Global H-mode Confinement Database, http://efdasql.ipp.mpg.de/hmodepublic/
[7] ITER Physics Expert Groups on Confinement and Transport and Confinement Modelling and Database *et al.,* Nucl. Fusion **39**, 2175 (1999).
[8] M. Kotschenreuther *et al.,* Comput. Phys. Commun. **88**, 128 (1995). Source program is downloaded from http://www.gs2.sourceforge.net/
[9] W. Dorland *et al.,* Phys. Rev. Lett. **85**, 5579 (2000).
[10] B.A. Trubnikov, *in Reviews of Plasma Physics*, edited by

M.A. Leontovich (Consultants Bureau, New York, 1965) Vol.1, pp.105-204.
[11] J.E. Kinsey *et al.,* Phys. Plasmas **13**, 022305 (2006).
[12] H. Nordman *et al.,* Plasma Phys. Control. Fusion **49**, 985 (2007).
[13] J.W. Connor *et al.,* Phys. Rev. Lett. **40**, 396 (1978).
[14] The ITER 1D Modelling Working Group, Nucl. Fusion **40**, 1955 (2000).
[15] R.L. Miller *et al.,* Phys. Plasmas **5**, 973 (1998).
[16] F. Jenko *et al.,* Plasma Phys. Control. Fusion **47**, B195 (2005).
[17] A.M. Dimits *et al.,* Phys. Plasmas **7**, 969 (2000).
[18] C. Angioni *et al.,* Nucl. Fusion **44**, 827 (2004).
[19] E. Fable *et al.,* Plasma Phys. Control. Fusion **52**, 015007 (2010).
[20] L. Schmitz *et al.,* Nucl. Fusion **52**, 023003 (2012).
[21] S. Hamaguchi and W. Horton, Phys. Fluids B **2**, 1833 (1990).
[22] S.I. Braginskii, *in Reviews of Plasma Physics*, edited by M.A. Leontovich (Consultants Bureau, New York, 1965) Vol.1, pp.205-311.
[23] X. Lapillonne *et al.,* Phys. Plasmas **16**, 032308 (2009).
[24] R.E. Waltz *et al.,* Phys. Plasmas **14**, 056116 (2007).
[25] T. Goerler and F. Jenko, Phys. Rev. Lett. **100**, 185002 (2008).
[26] N. Hayashi and JT-60 Team, Phys. Plasmas **17**, 056112 (2010).
[27] R.E. Waltz *et al.,* Phys. Plasmas **4**, 2482 (1997).
[28] G.M. Staebler *et al.,* Phys. Plasmas **14**, 055909 (2007).